ASTROBIOLOGY
Volume 14, Number 3, 2014
© Mary Ann Liebert, Inc.
DOI: 10.1089/ast.2013.1116

Microscale Mapping of Alteration Conditions and Potential Biosignatures in Basaltic-Ultramafic Rocks on Early Earth and Beyond

Eugene G. Grosch,[1] Nicola McLoughlin,[1] Pierre Lanari,[2] Muriel Erambert,[3] and Olivier Vidal[4]

Abstract

Subseafloor environments preserved in Archean greenstone belts provide an analogue for investigating potential subsurface habitats on Mars. The *c.* 3.5–3.4 Ga pillow lava metabasalts of the mid-Archean Barberton greenstone belt, South Africa, have been argued to contain the earliest evidence for microbial subseafloor life. This includes candidate trace fossils in the form of titanite microtextures, and sulfur isotopic signatures of pyrite preserved in metabasaltic glass of the *c.* 3.472 Ga Hooggenoeg Formation. It has been contended that similar microtextures in altered martian basalts may represent potential extraterrestrial biosignatures of microbe-fluid-rock interaction. But despite numerous studies describing these putative early traces of life, a detailed metamorphic characterization of the microtextures and their host alteration conditions in the ancient pillow lava metabasites is lacking.

Here, we present a new nondestructive technique with which to study the *in situ* metamorphic alteration conditions associated with potential biosignatures in mafic-ultramafic rocks of the Hooggenoeg Formation. Our approach combines quantitative microscale compositional mapping by electron microprobe with inverse thermodynamic modeling to derive low-temperature chlorite crystallization conditions. We found that the titanite microtextures formed under subgreenschist to greenschist facies conditions. Two chlorite temperature groups were identified in the maps surrounding the titanite microtextures and record peak metamorphic conditions at $315 \pm 40°C$ ($XFe^{3+}_{(chlorite)} = 25–34\%$) and lower-temperature chlorite veins/microdomains at $T = 210 \pm 40°C$ (lower $XFe^{3+}_{(chlorite)} = 40–45\%$). These results provide the first metamorphic constraints in textural context on the Barberton titanite microtextures and thereby improve our understanding of the local preservation conditions of these potential biosignatures. We suggest that this approach may prove to be an important tool in future studies to assess the biogenicity of these earliest candidate traces of life on Earth. Furthermore, we propose that this mapping approach could also be used to investigate altered mafic-ultramafic extraterrestrial samples containing candidate biosignatures. Key Words: Biosignatures on early Earth and Mars—Mid-Archean metabasalts and serpentinites—Mapping low-temperature alteration—Chlorite—Phyllosilicates. Astrobiology 14, 216–228.

1. Introduction

Over the past two decades, numerous studies of the basaltic oceanic crust have postulated that microbes may be involved in the alteration of volcanic glass, which opens up the possibility of a new, unexplored habitat for life (*e.g.,* Thorseth *et al.,* 1995; Fisk *et al.,* 1998; Furnes *et al.,* 2001a; Bach and Edwards, 2003; McLoughlin *et al.,* 2011). Candidate biosignatures in these subseafloor environments include micron-sized bioalteration textures in metavolcanic glass (*e.g.,* Fisk *et al.*, 1998; Furnes *et al.,* 2001a), strongly fractionated sulfur isotope values in basalt-hosted sulfides (*e.g.,* Rouxel *et al.,* 2008), and phylogenetic evidence for abundant and metabolically diverse biomass (*e.g.,* Santelli *et al.*, 2008; Lever *et al.,* 2013). Similar investigations of partially altered ultramafic serpentinites have found microtunnels in olivine phenocrysts, strongly fractionated sulfur isotopes of sulfides, and genetic evidence that argues for

[1]Department of Earth Science and Centre for Geobiology, University of Bergen, Bergen, Norway.
[2]Institut für Geologie, Universität Bern, Bern, Switzerland.
[3]Department of Geosciences, University of Oslo, Oslo, Norway.
[4]CNRS, ISTerre, Université Grenoble, Grenoble, France.

bioalteration in a hydrogen-rich subseafloor environment (Alt and Shanks, 2006; Fisk *et al.,* 2006; Mason *et al.,* 2010). The concept of biologically mediated basaltic glass alteration has been extended back in time to pillow lavas of ophiolite terrains (Furnes *et al.,* 2001b, 2008) and ancient Archean greenstone belts (*e.g.,* Furnes *et al.,* 2004; Banerjee *et al.,* 2006; Fliegel *et al.,* 2010). These workers invoke a fluid-rock-microbe alteration model, whereby microbes etch the volcanic glass, creating microtunnels to access reduced species in the glass (*e.g.,* Fe, Mn) that are used in lithotrophic metabolisms with more oxidized compounds in circulating seawater (Staudigel *et al.,* 2008 and references therein). These hollow tubular microtextures found in recent volcanic glass have been morphologically compared to titanite microtextures in Archean greenschist facies metabasaltic glass, which have therefore been argued to represent the earliest traces of life on Earth, dating as far back as *c.* 3.45 Ga (*e.g.,* Furnes *et al.,* 2004; Banerjee *et al.,* 2006, 2007; Fliegel *et al.,* 2010).

The potential involvement of microbes in the hydrothermal alteration of basalts and ultramafic rocks has extended the available habitats for life on Earth into sub-oceanic settings and perhaps into a hypothesized ''deep biosphere'' on Mars (*e.g.,* Fisk and Giovannoni, 1999). Moreover, it has been suggested that the microtunnels, argued to form during the low-temperature alteration of volcanic glass, may be used as an analogue in the search for life in meteorites, metabasaltic glass from Mars, and perhaps other rocky planets in our solar system (*e.g.,* Fisk *et al.,* 2006; McLoughlin *et al.,* 2007; Izawa *et al.,* 2010).

Despite numerous studies of putative Archean bioalteration textures in pillow lava metavolcanic glass of the Barberton and other greenstone belts (*e.g.,* Banerjee *et al.,* 2006, 2007; Furnes *et al.,* 2008), there are currently no metamorphic constraints on these low-grade metabasaltic rocks, particularly on the microscale metamorphic conditions surrounding the titanite microtextures. In this study, we used electron microprobe X-ray images and the recently developed software XMapTools (Lanari *et al.,* 2013, 2014a) to quantify the metamorphic temperature and chemical conditions of low-grade mineral assemblages associated with the candidate biosignatures in altered pillow lavas of the Barberton greenstone belt (BGB), South Africa. We illustrate using chlorite, a commonly occurring clay group mineral in altered basalts and ultramafics, that this approach can provide insights into the mid-Archean hydrothermal history, as well as the preservation conditions of the candidate biosignatures. More generally, we propose that this *in situ* mapping technique may prove to be a useful approach to further understanding of low-temperature hydrothermal environments associated with altered basalt or ultramafic-hosted candidate biosignatures beyond early Earth, for instance in meteorites, or perhaps one day Mars sample return studies.

2. Geological Background and Sample Description

To illustrate the advantages of the quantitative microscale mapping approach, we present a case study from the mid-Archean (3.472–3.432 billion-year-old) pillow lava metabasites of the BGB, South Africa, that are argued to contain the earliest traces of subseafloor microbial life on Earth (Furnes *et al.,* 2004; Banerjee *et al.,* 2006; Fliegel *et al.,* 2010). These pillow lavas overlie the world-renowned serpentinized ultramafic komatiites of the *c.* 3.482 billion-year-old Komati Formation (Fig. 1 and map in Supplementary Fig. S1; Supplementary Data is available online at www.liebertonline.com/ast). Figure 1 shows a schematic model summarizing potential Archean subseafloor habitable environments in the BGB (*e.g.,* Hanor and Duchac, 1990; Hofmann and Bolhar, 2007; Hofmann and Harris, 2008; Hofmann, 2011; McLoughlin *et al.,* 2012). Low-temperature hydrothermal alteration involving the silicification of pillow lavas beneath seafloor sediments (*i.e.,* volcaniclastic cherts) has been proposed in the BGB (*e.g.,* Hofmann and Bolhar, 2007; Hofmann and Harris, 2008) and argued to provide conditions suitable for life *c.* 3.45 billion years ago (Walsh, 1992; Westall *et al.,* 2006b, 2011; Philippot *et al.,* 2009; Grosch and McLoughlin, 2013). A recent study has used hydrothermally altered basalts and ultramafic rocks from the BGB as a petrological analogue for altered martian basalts as part of an International Space Analogue Rockstore, to be used for calibration of instruments intended for martian missions (Bost *et al.,* 2013). In this context, we propose the metabasaltic-hosted candidate biosignatures of the mid-Archean BGB as a useful analogue for investigating low-temperature hydrothermal alteration environments preserved in the martian subsurface.

The size, shape, and distribution of the Hooggenoeg titanite microtextures has been compared to microtunnels in recent volcanic glass and argued to represent microbial microtunnels that were formed in the Archean subseafloor and subsequently infilled by metamorphic titanite growth during ocean-floor hydrothermal alteration (Furnes *et al.,* 2004; Banerjee *et al.,* 2006; Staudigel *et al.,* 2008; Fliegel *et al.,* 2010). A recent critical assessment by McLoughlin *et al.* (2012) of the titanite microtextures from the type locality in the BGB has revealed the absence of organic carbon linings in the titanite microtextures by using a high-resolution ion probe mapping technique (nanoSIMS). These new data question a key line of evidence previously used to support the biogenicity of the Archean titanite microtextures. On the other hand, microscopic sulfides (pyrite) disseminated in the titanite and in the metabasaltic matrix were found to record a wide range in, and extremely negative, $\delta^{34}S$ values, providing evidence for microbial sulfate reduction in the BGB Archean subseafloor environment.

Here, we focused on three samples—BG29, BG173, and BG196—from the upper Hooggenoeg Formation of the BGB, a $\sim$2700 m thick unit of predominantly basaltic lavas, which, near our study site on the eastern limb of the Onverwacht anticline, is unconformably overlain by $\sim$200 m of clastic sedimentary rocks of the 3.432 Ga Noisy Formation (see Grosch *et al.,* 2011 and Supplementary Fig. S1). Sample BG29 is a surface sample of a nonvesicular pillow lava rim from the banks of the Komati River and an outcrop known as the ''biomarker cliff'' approximately 151 m beneath the erosional unconformity at the top of the Hooggenoeg Formation (Supplementary Fig. S1). This is the original outcrop that yielded the microtextures of Furnes *et al.* (2004), and sample BG29 is a parallel slice cut from the same hand sample. The pillow lavas are little deformed with well-developed chilled margins of formerly glassy material that grade inward to a variolitic zone. A second

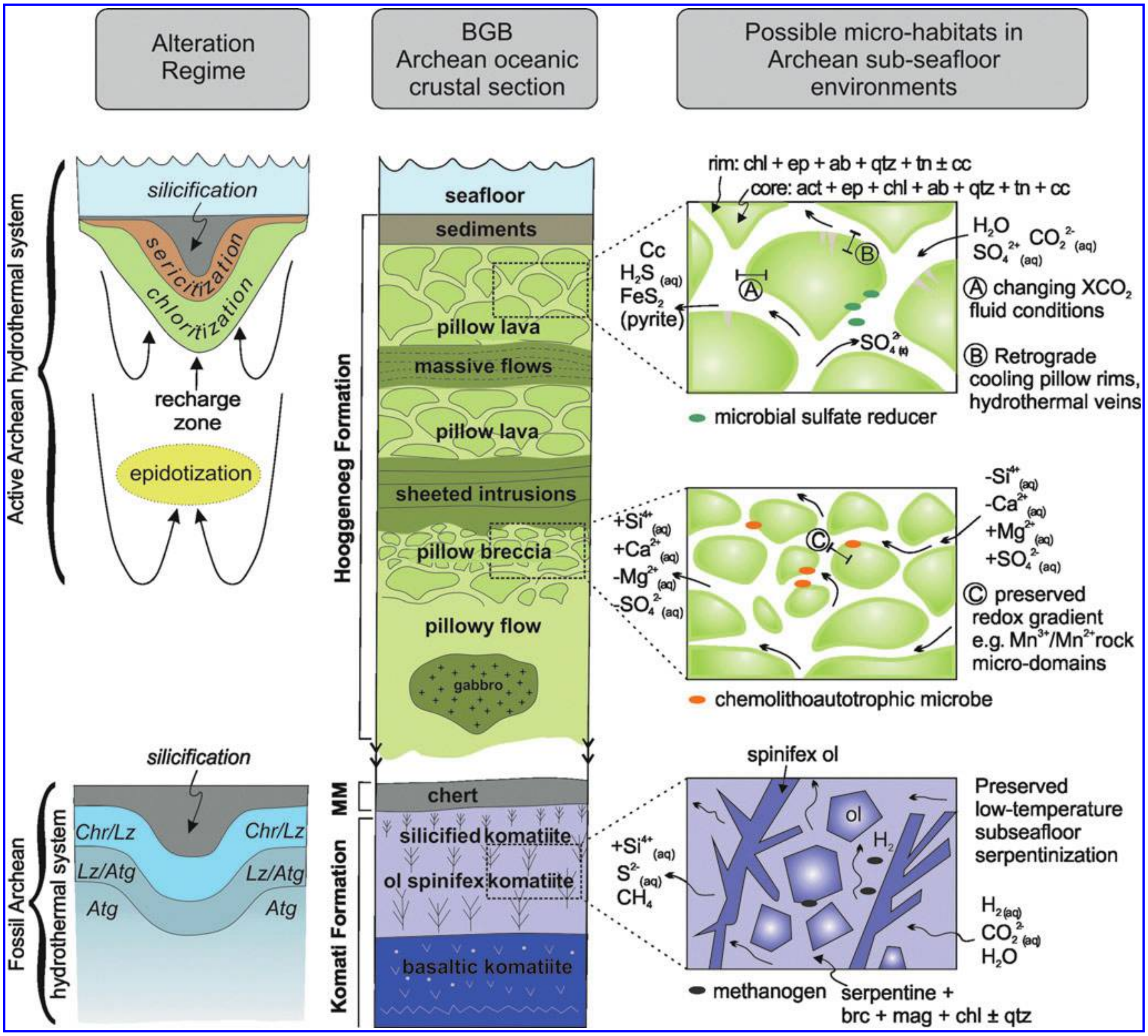

FIG. 1. Model of alteration regimes and potential habitats found in the Archean subseafloor that may have potentially supported fluid-rock-microbe interaction, shown as an analogue for possible microhabitats in the martian subsurface. Left-hand column shows an active hydrothermal alteration regime and a summary of the alteration minerals; lower part shows a fossil Archean hydrothermal system and alteration zones (Chr/Lz for chrysotile/lizardite, Lz/Atg for lizardite/antigorite). Central column shows the stratigraphy of an Archean oceanic crustal section preserved in the Onverwacht Group of the Barberton greenstone belt (BGB), South Africa, and the various lithologies found (MM, Middle Marker chert). Right-hand column expands on the potential microhabitats available for life in these Archean subseafloor niches. Top panel shows a pillow lava with the mineral phases found in core to rim, and circulating seawater containing putative sulfate-reducing microbes (after McLoughlin *et al.*, 2012). Central panel shows a pillow breccia with putative redox gradients that may have supported chemolithoautotrophic microbes. Lower panel postulates possible low-temperature subseafloor serpentinization in an olivine spinifex komatiite with hydrogen generation supporting putative methanogenic microbes.

surface sample, BG196, was also studied and represents a pillow lava core collected *c.* 200 m from the top of the pillow lava pile (see Supplementary Fig. S1). This upper part of the Hooggenoeg pillow lava sequence was also a target of the Barberton Scientific Drilling Project (BSDP) described by Grosch *et al.* (2009a, 2009b). Drill hole KD2b recovered 180 m of pillow lavas and a diabase intrusive with sample BG173, an interpillow hyaloclastite studied here (BG173), occurring at 147.7 m depth along the drill core (approx. 89 m from the top of the pillow lava pile).

Two metabasaltic pillow lava rim samples, BG29 and BG173, were selected for mapping of the titanite microtextures (Fig. 2a–2d), which occur as part of a chlorite ± quartz ± epidote ± calcite metavolcanic glass assemblage and are morphologically equivalent to the type microtextures described by Furnes *et al.* (2004). The titanite filaments

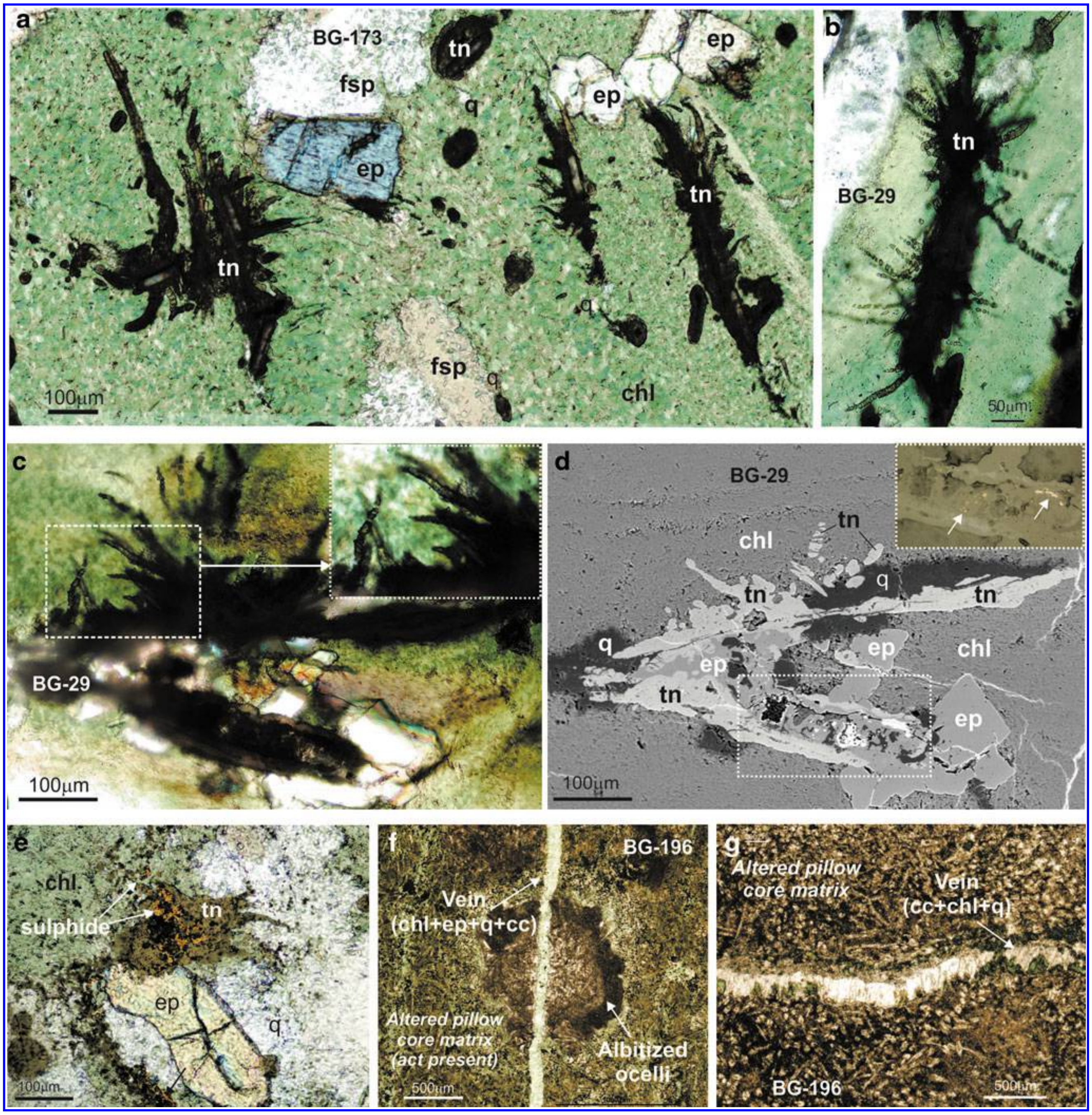

FIG. 2. (**a**) Alteration assemblage in pillow lava rim of sample BG173 corresponding to the area mapped by electron microprobe analysis. The candidate ''bioalteration'' titanite (tn) microtextures are shown occurring together with chlorite (chl), epidote (ep), feldspar (fsp), and quartz (q). (**b**, **c**) Petrographic transmitted light images of the original proposed bioalteration titanite microtextures in the sample BG29, described by Furnes *et al.* (2004). (**d**) Backscatter images of the area shown in (c) corresponding to the mapped area by electron microprobe analysis. Minute sulfides (pyrite, chalcopyrite arrowed) associated with the titanite-bearing alteration assemblage shown in top right inset (reflected light). (**e**) Sulfides (pyrite containing sulfur isotope biosignature) associated with the titanite microtextures in sample BG173. (**f**) Pillow core metabasalt sample containing albitized ocelli in a matrix of chlorite, quartz, epidote, with minor actinolite, titanite, and calcite. (**g**) Shows the very minor occurrence of calcite (cc), chlorite, quartz veins that occur in some places in the pillow core.

typically range from 2 to 40 μm in diameter, tens of micrometers long, are segmented by cross-cutting chlorite in some places. The titanite microfilaments project at both high and low angles and radiate from central cluster zones or bands of titanite (Fig. 2a–2d). Fine-grained sulfides, both pyrite and chalcopyrite, are found associated with the titanite (Fig. 2d, 2e; Fig. 3) also as coarse grain sulfides that occur in veins (Fig. 2e, Fig. 3, and McLoughlin *et al.,* 2012). The pillow lava core sample BG196 contains ocelli, a spherical magmatic quenching texture (Fig. 2f), in a matrix assemblage

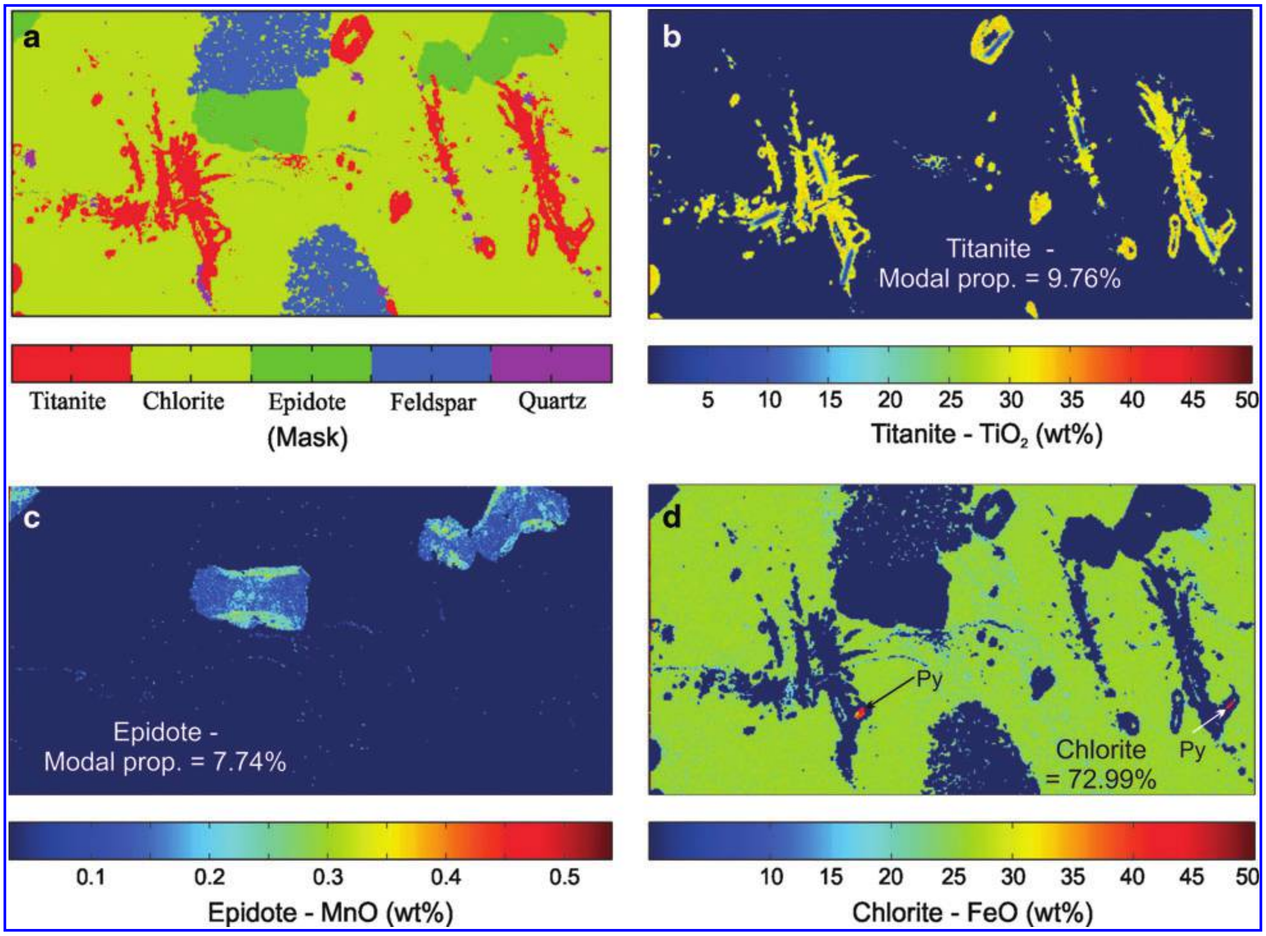

FIG. 3. (**a**) Mask file calculated with XMapTools, illustrating the pixels corresponding to each of the alteration minerals present. (**b**) Quantified map of the candidate titanite microtextures showing TiO_2 content and modal proportion of titanite in the map. (**c**) Quantified map of the epidote showing MnO composition (wt %), with MnO enrichment in rims, and modal proportion in map. (**d**) Quantified map of the chlorite matrix composition, also indicating pyrite (Py) grains present.

consisting of actinolite + chlorite + epidote + albite + quartz + trace amounts of accessory titanite and with minor cross-cutting chlorite-quartz-carbonate microveins in some places (Fig. 2f, 2g). This pillow lava core sample contains pseudomorphs of originally plagioclase-rich magmatic ocelli, now albitized.

3. Methodology

3.1. Microprobe mapping and data image processing

A Cameca SX100 electron microprobe with five wavelength-dispersive spectrometers (with LLIF, TAP, LTAP, PET, LPET WDS crystals selected for this study) at the Department of Geosciences, University of Oslo, was used to acquire point analyses and X-ray compositional maps. Two mid-Archean pillow metabasite samples, BG29 and BG173, were studied that include candidate titanite microtextures (Furnes *et al.,* 2004) and pyrite geochemical biosignatures (McLoughlin *et al.,* 2012; Grosch and McLoughlin, 2013). A total of nine X-ray compositional maps were derived from a single mapped area per sample in wavelength-dispersive mode that included the elements Si, Al, Ti, Fe, Mg, Mn, Ca, Na, and K. The compositional point analyses and maps were acquired in a technique similar to that described by De Andrade *et al.* (2006) and Lanari *et al.* (2012, 2013, 2014a). Point analyses also included profiles at high angles to mineral grain boundaries within the mapped area. Minerals used as analytical standards were natural wollastonite (Si, Ca), albite (Na), and orthoclase (K) and synthetic Al_2O_3, MgO, Cr_2O_3, and NiO. Pyrophanite (Mn, Ti) and Fe (metal) were used for instrument calibration. Analytical conditions for spot analyses were 15 keV accelerating voltage and 15 nA current. A higher current of 60–70 nA was used during the collection of map pixel data. The point analyses were then used as compositional standards to calibrate the nine qualitative X-ray elemental maps (see De Andrade *et al.,* 2006; Lanari *et al.,* 2014a). Representative mineral (point) compositional analyses for alteration phases in samples BG173 and BG29 are provided in Supplementary Table S1.

For the first map, sample BG173, an area of 1640 $\mu m \times 840$ μm was mapped out at 300 ms dwelling time per pixel, with a step size of 4 μm (resolution of 410 points by 210 rows). For the second map, sample BG29e, an area of 657 $\mu m \times 420$ μm was carried out at 300 ms dwelling time, with a 3 μm step size (resolution 220 points by 140 rows).

The raw X-ray compositional map data that include counts per pixel (X-ray element intensity) with map coordinates were treated by using a newly developed MATLAB-based software program, XMapTools (Lanari *et al.,* 2014a). This program identifies and displays the locations of the mapped mineral phases from the raw X-ray image data files and converts, by standardization, the raw qualitative map data into quantitative map pixel data by using mineral compositional point analyses (see Supplementary Fig. S2 and Lanari *et al.,* 2014a, for further detailed statistical discussion). One of the main advantages of this new mapping software is that small changes in mineral composition (and as a consequence their physicochemical conditions) on a microscale can be monitored and linked to textural information at the thin-section scale (Martin *et al.,* 2013; Lanari *et al.,* 2014a). The software allows for estimation of mineral modal proportions and the calculation of mineral structural formulae that can then be used in petrological calculations on the mapped assemblage.

3.2. Thermodynamic modeling and mineral chemistry

In this study, we focused mainly on the chlorite mineral group, given that this mineral is common in mafic and ultramafic rocks and known to be stable over a wide range of temperature and pressure conditions (*e.g.,* Vidal *et al.,* 2001, 2005, 2006; Grosch *et al.,* 2012; Lanari *et al.,* 2014b). As a first step, we applied the empirical chlorite geothermometers of Cathelineau (1988) and Hillier and Velde (1991) to the maps. These empirical chlorite temperature maps are calculated from Al(iv) and Si content in the tetrahedral T_1 site of the chlorite at each pixel, and the results are summarized in Supplementary Fig. S3 (a–d). It is important, however, to note that some workers have questioned the reliability of empirical chlorite geothermometers for a number of crystal-chemical reasons (de Caritat *et al.,* 1993; Jiang *et al.,* 1994). Application of the more recently proposed chlorite geothermometer of Inoue *et al.* (2009) to the BG173 chlorite compositional map is also presented (Supplementary Fig. S3c, S3d). It is illustrated that calculated chlorite temperature estimates derived using this geothermometer are sensitive to small changes in arbitrarily chosen values of XFe^{3+} chlorite content (*e.g.,* at $XFe^{3+} = 15\%$ and $XFe^{3+} = 30\%$), resulting in apparent shifts of peak metamorphic chlorite crystallization conditions of up to ~ 100°C. As a final step, we applied the inverse thermodynamic modeling approach involving chlorite-quartz-water equilibria (Vidal *et al.,* 2001, 2005, 2006), using the composition of chlorite from each 3-micron pixel in the mapped area to calculate a metamorphic chlorite crystallization temperature and an estimate of XFe^{3+} at each pixel in the map. Vidal *et al.* (2006) and Muñoz *et al.* (2006) provided detailed explanations of the chlorite thermodynamic modeling approach involving simultaneous estimation of chlorite temperature and chlorite XFe^{3+} content. Grosch *et al.* (2012) offered an example of this thermodynamic approach applied to a wide range of low-temperature Archean metabasites.

4. Results

A general map of the metamorphic mineral phases in sample BG173 from a pillow lava rim is presented in the mask image calculated by XMapTools (Fig. 3a). The low-temperature and low-pressure metamorphic alteration assemblage in this metavolcanic glass sample includes chlorite ($(Mg,Fe)_3(Si,Al)_4O_{10}(OH)_2 \cdot (Mg,Fe)_3(OH)_6$), titanite ($CaTiSiO_5$), feldspar ($KAlSi_3O_8$–$NaAlSi_3O_8$–$CaAl_2Si_2O_8$), epidote ($Ca_2Al_2(Fe^{3+};Al)(SiO_4)(Si_2O_7)O(OH)$), and quartz ($SiO_2$). Separate image maps are shown for selected mineral phases with major element compositions given in weight percent (Fig. 3b–3d). The titanite, for example, shows a restricted range in TiO_2 content of between 30 and 34 wt %, whereas chlorite composition varies significantly, as indicated in FeO content between 18 and 28 wt %. The epidote compositional map shows microscale variation in MnO wt %, with high MnO content in the epidote rims (Fig. 3c), indicating Mn (Mn^{2+}, Mn^{3+}) enrichment in the epidote crystal structure. The modal proportions of each phase can also be estimated from the pixel images. Modal proportions of the mineral phases present in the mapped image are (a) chlorite = 72.9%, (b) titanite = 9.8%, feldspar = 8.6%, epidote = 7.7%, and quartz represents approximately 2% (Fig. 3b–3d). It is also possible to calculate the local rock composition from the mapped area containing the metavolcanic-hosted candidate biosignature(s) (see Supplementary Table S1 for BG173), allowing for assessment of local chemical variations in rock composition.

To derive reliable chlorite metamorphic temperature estimates in the map for sample BG173 and to simultaneously constrain the XFe^{3+} content of chlorite, we applied the thermodynamic modeling approach that involves the convergence criteria of chlorite-quartz-water equilibria (Vidal *et al.,* 2005, 2006) to the chlorite map. The calculated mineral, chemical, and metamorphic data results are shown in the maps in Fig. 4a, 4b. The temperature distribution calculated from each chlorite pixel composition is shown along with estimated Al(iv) content of the chlorite in Fig. 4c–4e. The histogram for all pixel temperature estimates indicates a peak metamorphic chlorite temperature estimate at $T = 315 \pm 30$°C (Fig. 4d). Although a continuous spread in estimated temperature is shown in the Al(iv) versus temperature plot (Fig. 4c), close inspection of the map in Fig. 4a shows the microtextural occurrence of two chlorite temperature populations, due to compositional changes. Although most of the chlorite pixels in the map background record a temperature range of between 280°C and 350°C, some lower-temperature subparallel chlorite bands are observed recording conditions of between 140°C and 225°C (see top right corner of map in Fig. 4a). These lower-temperature bands are also associated with higher estimates of XFe^{3+} content in chlorite (Fig. 4b). Thus, two chlorite population groups are identified, namely, peak metamorphic conditions at 315 ± 40°C ($XFe^{3+}_{(chlorite)} = 25$–$34\%$) and lower-temperature microbands recording conditions of $T = 210 \pm 40$°C (lower $XFe^{3+}_{(chlorite)} = 40$–$45\%$). Lower-temperature chlorite bands are also indicated in the temperature maps calculated by using the Cathelineau (1988) and the Hillier and Velde (1991) empirical geothermometers (Supplementary Fig. S3a, S3b). Similarly, independent of chosen XFe^{3+} content in chlorite (at both $XFe^{3+} = 15\%$ and $XFe^{3+} = 30\%$), application of the Inoue *et al.* (2009) geothermometer to the maps also reveals low- and high-temperature bands (see Supplementary Fig. S3c, S3d).

Metamorphic temperature estimates were calculated for each pixel in the second sample map BG29, from the type

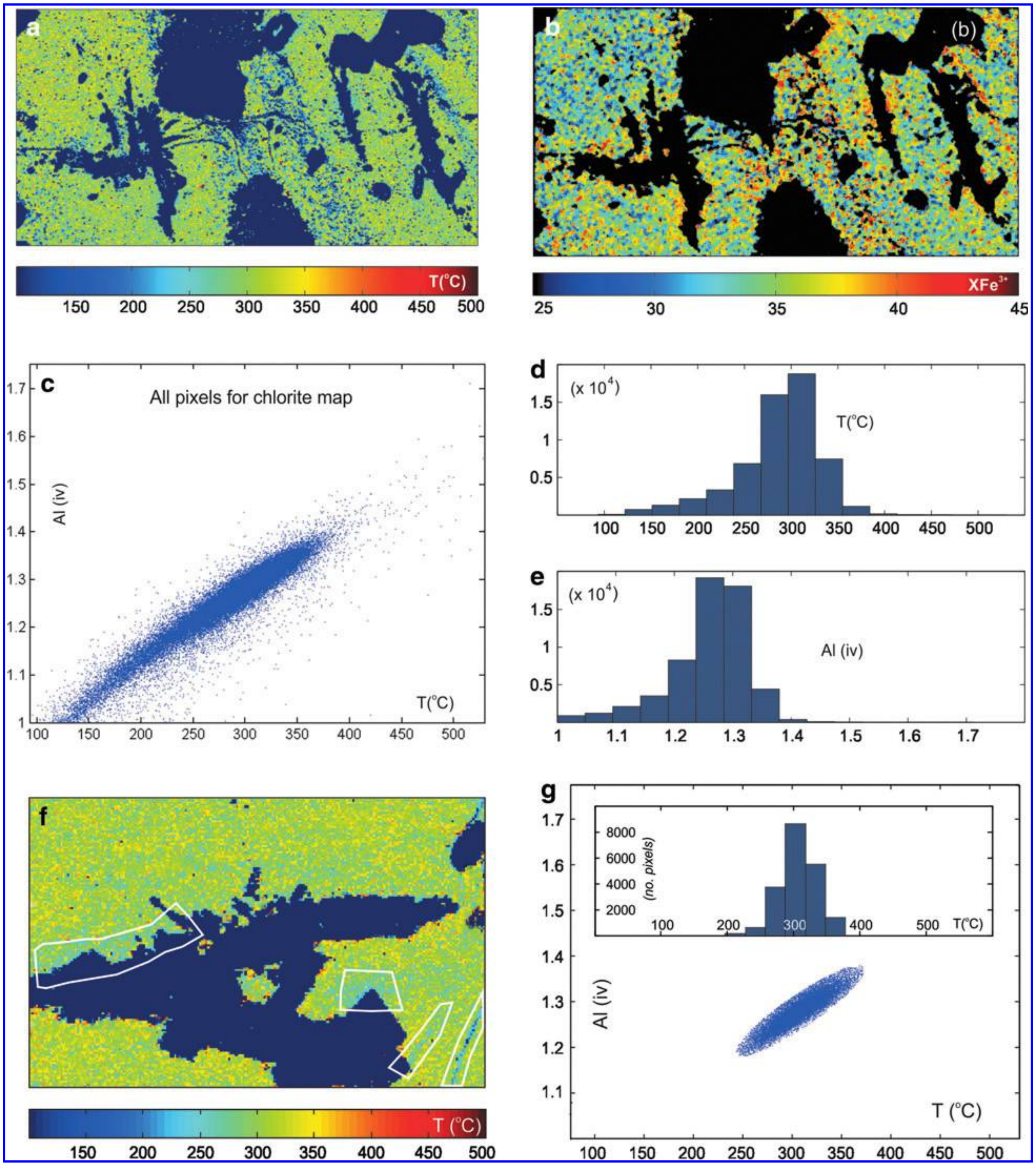

FIG. 4. Application of the chlorite-quartz-water inverse thermodynamic approach of Vidal *et al.* (2001, 2006) to the chlorite map in BG173 and BG29e that estimates (**a**) chlorite crystallization temperature from each compositional pixel and (**b**) minimum XFe^{3+} in chlorite. (**c**) A binary plot showing temperature estimates from each pixel and estimate of Al(iv) content of chlorite. (**d**) Histogram showing all temperature estimates from chlorite compositional pixels in BG173. (**e**) Histogram of Al(iv) content of chlorite from each pixel of the map in BG173, (**f**) pixel temperature map for candidate biosignature sample BG29e, and (**g**) pixel distribution of calculated chlorite temperature versus Al(iv) chlorite content in a binary plot derived from the quantitative chlorite map in sample BG29e; inset shows a histogram of the calculated chlorite temperature estimates.

sample of Furnes *et al.* (2004), also by using the chlorite-quartz-water thermodynamic modeling approach. The calculated results are shown in Fig. 4f, 4g. The mapped area represents compositional pixels in a chlorite matrix surrounding a reaction texture consisting of epidote, titanite, and quartz (in black), as highlighted in the petrography Section 2 (Fig. 2d, 2e). The metamorphic map presented in Fig. 4f, 4g records chlorite crystallization temperatures surrounding the titanite microtextures previously argued by Furnes *et al.* (2004) and Fliegel *et al.* (2010) to represent an

Archean morphological biosignature and the earliest trace fossil on Earth. The distribution in pixels in a plot of Al(iv) versus calculated chlorite crystallization temperature indicates alteration conditions centered on $T = 305 \pm 30°C$, with a few lower-temperature microdomains and veins recording $T = 260 \pm 30°C$ (see white outlined boxes in Fig. 4f and histogram in Fig. 4g).

5. Discussion

5.1. Metamorphic constraints on candidate mid-Archean bioalteration textures

The mapping approach presented here allowed us to monitor microscale variations in alteration mineral chemistry and obtain reliable estimates of metamorphic conditions preserved around candidate biosignatures in the hydrothermally altered mid-Archean pillow lava pile. These constraints are important because local and microscale metamorphic data on Earth's earliest proposed candidate ''bioalteration'' textures (*e.g.,* Furnes *et al.,* 2004) and early pyrite isotopic biosignatures (McLoughlin *et al.,* 2012; Grosch and McLoughlin, 2013) is lacking.

The metamorphic temperature results in the actinolite-absent metavolcanic pillow lava rims (BG173 and BG29; $T = 315–210°C$), combined with the occurrence of actinolite only in the pillow core sample (BG196), indicate that hydrothermal alteration occurred over a range of low-temperature fluid conditions from subgreenschist to transitional greenschist facies conditions. Pillow lava metabasaltic rims have actinolite-absent, titanite-epidote-quartz-rich alteration assemblages. Peak metamorphic conditions in the rims occurred at around $T = 315 \pm 30°C$, with later stage retrograde fluid veining at around 210°C. These two metamorphic events may have taken place under different fluid redox conditions, namely, lower oxygen fugacity ($XFe^{3+}_{(chlorite)} = 25–34\%$) at the peak of metamorphism to lower-temperature, high oxygen fugacity conditions (lower $XFe^{3+}_{(chlorite)} = 40–45\%$) for the later event. Changes in fluid chemistry are also recorded in epidote core-rim composition, with Mn^{2+} enrichment in epidote rims. Thus, we argue for changing redox conditions of the metamorphic fluid during alteration and cooling in the pillow rims, and document a potential redox gradient preserved on a microscale in the Archean subseafloor environment, which may have been exploited by early subseafloor endolithic microorganisms (*cf.* McLoughlin *et al.,* 2011).

In the bioalteration model of Furnes *et al.* (2004) and Banerjee *et al.* (2006), it is argued that growth of titanite occurred in an early subseafloor greenschist facies hydrothermal alteration regime. We argue that titanite formation was not restricted to conditions in the greenschist facies and that it is more likely that the titanite microtextures formed under low-temperature subgreenschist facies–transitional greenschist facies conditions in the pillow lava rims. An *in situ* U-Pb geochronological age constraint on titanite growth in the altered Hooggenoeg pillow lavas (Fliegel *et al.,* 2010) has been estimated at 3.334 ± 0.058 Ga, but this age falls midway between the estimated age of seafloor alteration at 3.482 Ga (Ar-Ar age data of Lopez-Martinez *et al.,* 1992) and tectono-thermal activity at 3.223 Ga (*e.g.,* Moyen *et al.,* 2006), regionally accepted in this part of the greenstone belt. Given these U-Pb age discrepancies on the timing of alteration and the possibility of different low-temperature metamorphic events reported here, we argue that further high-resolution quantitative mapping is required to test the syngenicity and biogenicity of the titanite microtextures and the origin of the metamorphic fluids.

5.2. Application to alteration and potential biosignatures in extraterrestrial rocks

Recent orbital remote sensing missions and Mars rover observations have found evidence for extensive low-temperature surface and subsurface alteration of ancient basaltic lavas on Mars (*e.g.,* Ehlmann *et al.,* 2011a, 2011b, 2013; Squyres *et al.,* 2012; Bishop *et al.,* 2013a; Michalski *et al.,* 2013). These studies report *in situ* and hyperspectral data in support of the relatively common occurrence of (Fe, Mg)-rich phyllosilicates (*e.g.,* chlorite, smectite, and serpentine) and Al-rich phyllosilicates (kaolin, montmorillonite) on the exposed surface of Mars. Other alteration minerals and weathering products such as illite, mica, zeolites (analcime), carbonates, sulfates, and quartz in silicified basalts have been reported (*e.g.,* Squyres *et al.,* 2008; Bishop *et al.,* 2013a; Ehlmann *et al.*, 2013). A schematic summary diagram of the surface and subsurface environments on Mars showing various locations where clay minerals and carbonates have been identified in basalts and ultramafic rocks is shown in Fig. 5a–5e, as compiled from recent hyperspectral data and inferred geological settings (Carr and Head, 2010; Ehlmann *et al.,* 2011a, 2011b, 2013; Squyres *et al.,* 2012; Bishop *et al.,* 2013a, 2013b; Michalski *et al.,* 2013). Also shown in Fig. 5f–5k are hypothetical examples of a range of possible biosignatures that may be found in extraterrestrial metabasaltic and serpentinized ultramafic rocks. In this context, we propose that the new mapping approach on Archean metabasaltic samples presented herein may potentially be applied to aqueously altered martian basaltic and ultramafic rocks containing candidate biosignatures.

Crustal clays including chlorite have been reported in the oldest central parts of craters and argued to represent subsurface hydrothermal alteration prior to 3.7 Ga during the Noachian, when Mars had an arid, cold surface climate (Fig. 5a; Ehlmann *et al.,* 2011a, 2011b, 2013). These authors argue that possible early life may have been restricted to warm hydrothermal environments of the basaltic/ultramafic subsurface. Potential morphological and mineral-chemical biosignatures suggested from these environments include mineralized microtunnels in metavolcanic glass (McLoughlin *et al.,* 2007 and references therein) and putative hyphae in vesicular metabasalts (Cavalazzi *et al.,* 2011; McMahon *et al.,* 2013), and these are shown in Fig. 5f–5h. In contrast, Bishop *et al.* (2013a) argued that low-temperature clay formation in > 3.7 Ga basalts may be due to both early subsurface alteration and near-surface hydrothermal alteration resulting from impact metamorphism. Bishop *et al.* (2013a) also reported the widespread occurrence of saponite and beidellite smectite clays in ancient exposed central parts of basaltic craters. Post-impact hydrothermal systems have been argued to provide suitable environments for early microorganisms to thrive (*e.g.,* Cockell, 2006; Squyres *et al.,* 2012). Potential biosignatures in mafic-ultramafic impact settings include the sulfur isotope fractionation of hydrothermal sulfides (Fig. 5j; Parnell *et al.,* 2010b), and organic biomarkers (*e.g.,* Parnell *et al.,* 2007).

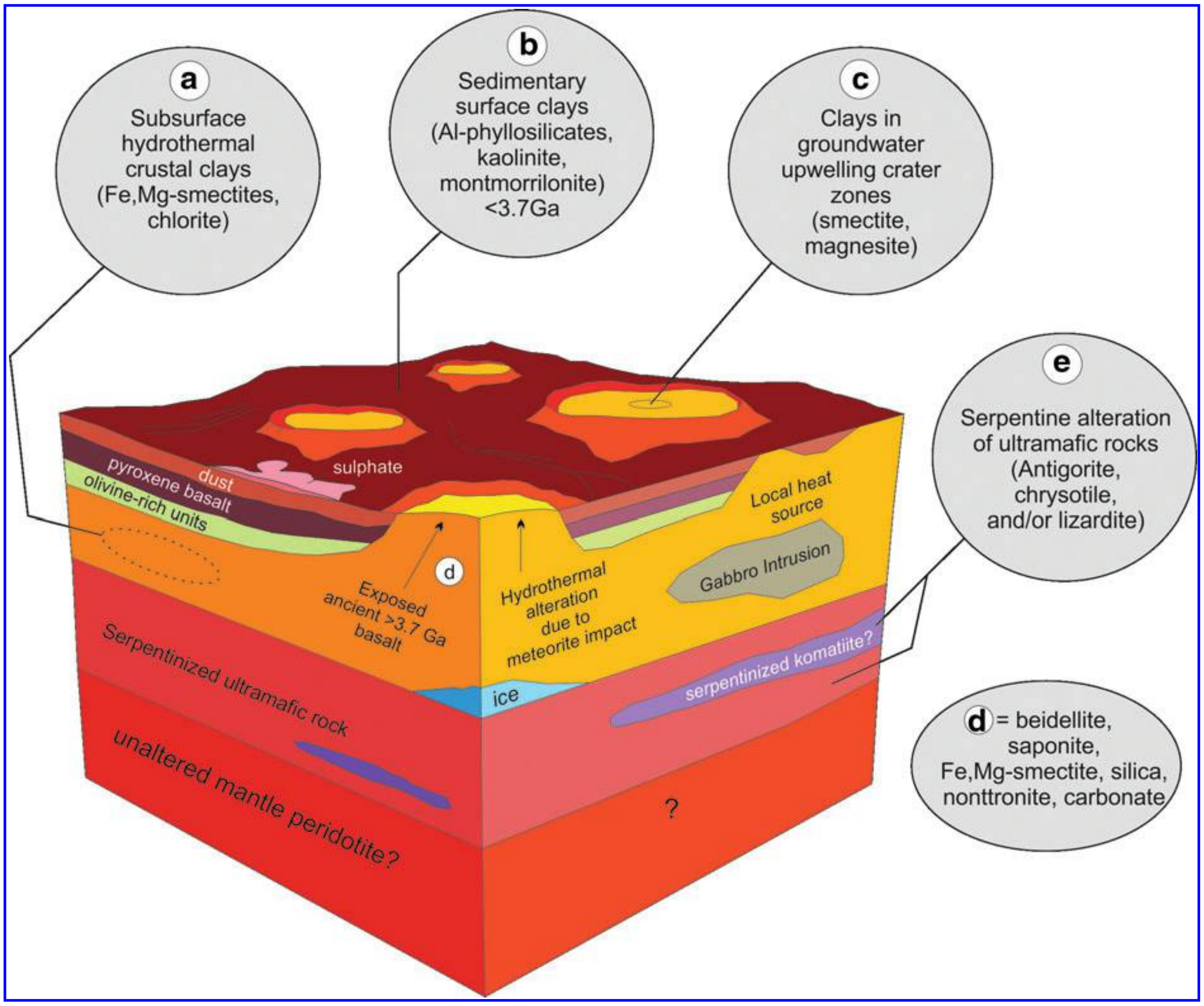

FIG. 5. Schematic diagram of the surface and subsurface of Mars. Upper panel shows a range of environments with clay mineral and phyllosilicate formation; lower panel shows the range of candidate biosignatures that may be found in these environments. Upper panel: (**a** and **b**) after remote sensing data of Ehlmann *et al.* (2013), showing crustal and sedimentary surface clays. (**c**) Clays identified in McLaughlin Crater indicating alkaline groundwater activity in shallow subsurface on Mars (see Michalski *et al.,* 2013). (**d**) Ancient <3.7 Ga exposed basalts in crater centers formed during hydrothermal alteration in a postmeteorite impact setting or other subsurface low-temperature alteration processes (Bishop *et al.,* 2013a). (**e**) Serpentinization in ultramafic rocks on Mars (*e.g.,* possible subsurface komatiites) resulting in release of subsurface hydrogen (*e.g.,* see Oze and Sharma, 2005). Lower panel shows alteration phases and potential biosignatures found in (**f**) altered pillow lava metavolcanic glass with microtubular candidate bioalteration textures; (**g**) altered hyaloclastite (glassy breccia) containing candidate microtubular bioalteration textures on the rims of altered glass fragments; (**h**) vesicular lava containing sulfides that could preserve a biogenic $\delta^{34}S$ signature, also endolithic hyphae in mineralized vesicles; (**i**) metavolcanic glass containing the titanite microtextures of argued biogenic origin studies herein; (**j**) metabasaltic/metagabbroic impact breccia containing sulfides recording a $\delta^{34}S$ signature of a putative post-impact hydrothermal microbial ecosystem; (**k**) an ultramafic metadunite containing tubular alteration textures in fracture olivines. Textural sketches of potential basalt/ultramafic-hosted biosignatures modified after (f) Furnes *et al.* (2001a); (g) Cousins *et al.* (2009), Banerjee and Muehlenbachs (2003); (h) Peckmann *et al.* (2008), Schumann *et al.* (2004), Cavalazzi *et al.* (2011), McMahon *et al.* (2013); (i) Furnes *et al.* (2004), Banerjee *et al.* (2006), Staudigel *et al.* (2008); (j) Parnell *et al.* (2010a, 2010b), Cockell (2006); (k) Fisk *et al.* (2006). Mineral abbreviations: zeol = zeolite, pal = palagonite, beid = beidellite, sap = saponite, pheno = phenocryst, qtz = quartz, cc = calcite/carbonate, ep = epidote, tn = titanite, py = pyrite, ol = olivine, serp = serpentine, idns = iddingsite.

The occurrence of serpentine alteration phases on Mars (*e.g.,* Bishop *et al.,* 2013a) and the detection of methane in the martian atmosphere have also been taken by some workers to suggest the possibility of serpentinization (Oze and Sharma, 2005) that could fuel (or may have fueled) a subsurface chemosynthetic biosphere through the generation of hydrogen and/or methane (*e.g.,* Schulte *et al.,* 2006; Hellevang *et al.,* 2010; McCollom and Seewald, 2013). A number of potential biosignatures have been proposed for serpentinites, which on Mars could include microtunnels in olivines (Fisk *et al.,* 2006; Fig. 5k), sulfides with pronounced $\delta^{34}S$ signatures (*cf.* Alt and Shanks, 2006), organic-bearing fluid inclusions (Parnell *et al.,* 2010a), and organic compounds (Delacour *et al.,* 2008; Ménez *et al.,* 2012), summarized in

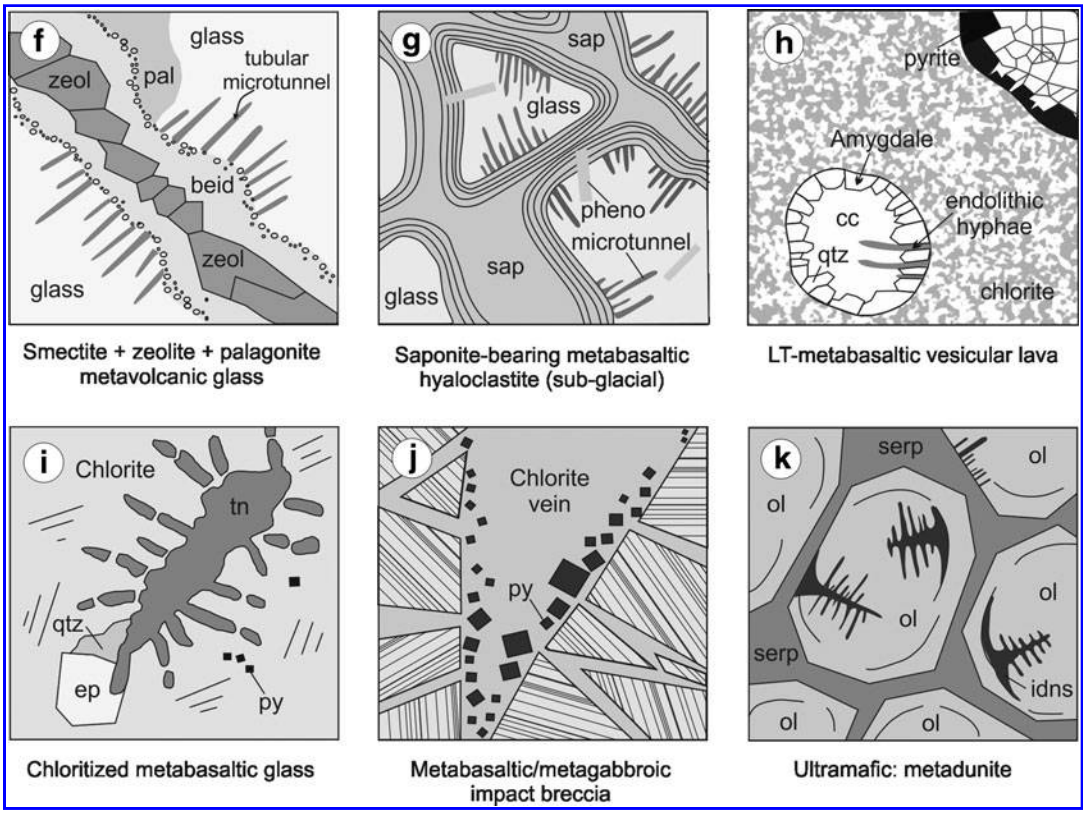

FIG. 5. (Continued).

Fig. 5. One of the advantages of the approach presented here is that it is a nondestructive technique, so a valuable sample such as a martian serpentine-bearing meteorite does not need to be powdered, which allows the candidate biosignature to be investigated in textural context along with microscale variations in serpentine composition (*cf.* Fisk *et al.,* 2006; Fig. 5k). In addition, changes in ''effective'' or local bulk rock composition can be calculated from the mapped area (see Supplementary Table S1 for BG173) and used for phase diagram modeling. This approach can be combined with other *in situ* techniques, such as XANES mapping of iron speciation (redox conditions) in clay minerals (*e.g.,* De Andrade *et al.,* 2006; Muñoz *et al.,* 2006) and Raman spectroscopy and/or micro-X-ray diffraction to investigate the sequence of alteration events, physicochemical conditions, and the preservation environment of candidate extraterrestrial biosignatures.

6. Conclusions

In this study, we applied a quantitative electron microprobe mapping approach to investigate altered metabasaltic pillow lavas from the mid-Archean Barberton greenstone belt, which is argued to contain morphological and mineral-chemical biosignatures (Furnes *et al.,* 2004; McLoughlin *et al.,* 2012). This nondestructive mapping approach allowed us to (i) estimate the modal proportions of titanite microtextures and surrounding alteration mineral phases (Fig. 3), (ii) evaluate microscale compositional changes in alteration minerals associated with candidate biosignatures, (iii) calculate metamorphic temperature variations on the thin-section scale in two-dimensional space (Fig. 4), and (iv) calculate changes in the local rock composition of the mapped area containing the candidate biosignature. Taken together, this petrological information provides new constraints on the ancient alteration environment in the pillow lava sequence and the preservation conditions of the candidate biosignatures (Figs. 3 and 4).

Petrographic observations and the quantitative mapping results indicate that metamorphic alteration in the Barberton pillow lava metabasalts occurred near the subgreenschist to greenschist facies boundary, with temperatures of between 210°C and 315°C. We also report the possible preservation of a hydrothermal redox gradient due to a changing low-temperature fluid composition (Fig. 3c, Fig. 4b). We propose that this microscale mapping approach in conjunction with *in situ* geochronological methods holds much potential to further assess the syngenicity and biogenicity of titanite microtextures from the mid-Archean BGB and other greenstone belt or ophiolite terrains.

We also explore the scope of this mapping approach for understanding low-temperature alteration conditions in extraterrestrial metabasalts, metagabbros, and serpentinized ultramafic rocks, including meteorites. We postulate that this approach may help to constrain environmental conditions in possible habitable zones in basaltic-ultramafic rocks in the Solar System (Fig. 5). On Mars, low-temperature hydrothermally altered rocks have been identified as a priority target for sample return (*e.g.,* McLennan *et al.,* 2012), and the approach presented here may help to assess the preservation conditions of potential biosignatures (Fig. 5f–5k) in the martian subsurface.

Acknowledgments

This project was financially supported by the Norwegian Research Council through the Centre for Geobiology to E.G and N.M, also by Bergens Forskningsstiftelse (BFS) and UiB.

Abbreviation

BGB, Barberton greenstone belt.

References

Alt, J.C. and Shanks, W.C. (2006) Stable isotope compositions of serpentinite seamounts in the Mariana forearc: serpentinization processes, fluid sources and sulfur metasomatism. *Earth Planet Sci Lett* 242:272–285.

Bach, W. and Edwards, K.J. (2003) Iron and sulphide oxidation within the basaltic ocean crust: implications for chemolithoautotrophic microbial biomass production. *Geochim Cosmochim Acta* 67:3871–3887.

Banerjee, N.R. and Muehlenbachs, K. (2003) Tuff life: bioalteration in volcaniclastic rocks from the Ontong Java Plateau. *Geochemistry, Geophysics, Geosystems* 4, doi:1029/2002GC000470.

Banerjee, N.R., Furnes, H., Muehlenbachs, K., Staudigel, H., and de Wit, M. (2006) Preservation of *c.* 3.4–3.5 Ga microbial biomarkers in pillow lavas and haloclastites from the Barberton greenstone belt, South Africa. *Earth Planet Sci Lett* 241:707–722.

Banerjee, N.R., Simonetti, A., Furnes, H., Muehlenbachs, K., Staudigel, H., Heaman, L., and Van Kranendonk, M.J. (2007) Direct dating of Archean microbial ichnofossils. *Geology* 35:487–490.

Bishop, J.L., Tirsch, D., Tornabene, L.L., Jaumann, R., McEwen, A.S., McGuire, P.C., Ody, A., Poulet, F., Clark, R.N., Parente, M., McKeown, N.K., Mustard, J.F., Murchie, S.L., Voigt, J., Aydin, Z., Bamberg, M., Petau, A., Michael, G., Seelos, F.P., Hash, C.D., Swayze, G.A., and Neukum, G. (2013a) Mineralogy and morphology of geological units at Libya Montes, Mars: ancient aqueously derived outcrops, mafic flows, fluvial features, and impacts. *J Geophys Res: Planets* 118:487–513.

Bishop, J.L., Loizeau, D., McKeown, N.K., Saper, L., Dyar, M.D., Des Marais, D.J., Parente, M., and Murchie, S.L. (2013b) What the ancient phyllosilicates at Mawrth Vallis can tell us about possible habitability on early Mars. *Planet Space Sci* 86:130–149.

Bost, N., Westall, F., Ramboz, C., Fouchera, F., Pullan, D., Meunier, A., Petit, S., Fleischer, I., Klingelhöfer, G., and Vago, J.L. (2013) Missions to Mars: characterisation of Mars analogue rocks for the International Space Analogue Rockstore (ISAR). *Planet Space Sci* 82–83:113–127.

Carr, M.H. and Head, J.W., III. (2010) Geologic history of Mars. *Earth Planet Sci Lett* 294:185–203.

Castaing, R. (1951) *Application des sondes electronique a une methode d'analyse ponctuelle chimique et cristallographique,* Université de Paris (publication ONERA), Paris.

Cathelineau, M. (1988) Cation site occupancy in chlorites and illites as a function of temperature. *Clay Miner* 23:471–485.

Cavalazzi, B., Westall, F., Cady, S.L., Barbieri, R., and Foucher, F. (2011) Potential fossil endoliths in vesicular pillow basalt, Coral Patch Seamount, eastern North Atlantic Ocean. *Astrobiology* 11:619–632.

Cockell, C.S. (2006) The origin and emergence of life under impact bombardment. *Philos Trans R Soc Lond B Biol Sci* 361:1845–1856.

Cousins, C.R., Smellie, J.L., Jones, A.P., and Crawford, I.A. (2009) A comparative study of endolithic microborings in basaltic lavas from a transitional subglacial–marine environment. *International Journal of Astrobiology* 8:37–49.

De Andrade, V., Vidal, O., Lewin, E., O'Brien, P., and Agard, P. (2006) Quantification of electron microprobe compositional maps of rock thin sections: an optimized method and examples. *Journal of Metamorphic Geology* 24:655–668.

de Caritat, P., Hutcheon, I., and Walshe, J.L. (1993) Chlorite geothermometry: a review. *Clays Clay Miner* 41:219–239.

Delacour, A., Fruh-Green, G.L., Bernasconi, S.M., Schaeffer, P., and Kelley, D.S. (2008) Carbon geochemistry of serpentinites in the Lost City Hydrothermal System (30°N, MAR). *Geochim Cosmochim Acta* 72:3681–3702.

Ehlmann, B.L., Mustard, J.F., Murchie, S.L., Bibring, J.P., Meunier, A., Fraeman, A.A., and Langevin, Y. (2011a) Subsurface water and clay mineral formation during the early history of Mars. *Nature* 479:53–60.

Ehlmann, B.L., Mustard, J.F., Clark, R.N., Swayze, G.A., and Murchie, S.L. (2011b) Evidence for low-grade metamorphism, diagenesis, and hydrothermal alteration on Mars from phyllosilicate mineral assemblages. *Clays Clay Miner* 59:359–377.

Ehlmann, B.L., Mustard, J.F., Murchie, S.L., Bibring, J.-P., Meunier, A., Fraeman, A.A., and Langevin, Y. (2013) Geochemical consequences of widespread clay mineral formation in Mars' ancient crust. *Space Sci Rev* 174:329–364.

Fisk, M.R. and Giovannoni, S.J. (1999) Sources of nutrients and energy for a deep biosphere on Mars. *J Geophys Res* 104:11805–11815.

Fisk, M.R., Giovannoni, S.J., and Thorseth, I.H. (1998) Alteration of oceanic volcanic glass: textural evidence of microbial activity. *Science* 281:978–980.

Fisk, M.R., Popa, R., Mason, O.U., Storrie-Lombardie, M.C., and Vicenzi, E.P. (2006) Iron-magnesium silicate bioweathering on Earth (and Mars?). *Astrobiology* 6:48–68.

Fliegel, D., Kosler, J., McLoughlin, N., Simonetti, A., de Wit, M.J., Wirth, R., and Furnes, H. (2010) *In situ* dating of Earth's oldest trace fossil at 3.34 Ga. *Earth Planet Sci Lett* 299:290–298.

Furnes, H., Staudigel, H., Thorseth, I.H., Torsvik, T., Muehlenbachs, K., and Tumyr, O. (2001a) Bioalteration of basaltic glass in the oceanic crust. *Geochemistry, Geophysics, Geosystems* 2, doi:10.1029/2000GC000150.

Furnes, H., Muehlenbachs, K., Tumyr, O., Torsvik, T., and Xenophontos, C. (2001b) Biogenic alteration of volcanic glass from the Troodos ophiolite, Cyprus. *J Geol Soc London* 158:75–84.

Furnes, H., Banerjee, N.R., Muehlenbachs, K., Staudigel, H., and de Wit, M. (2004) Early life recorded in Archaean pillow lavas. *Science* 304:578–581.

Furnes, H., McLoughlin, N., Muehlenbachs, K., Banerjee, N.R., Staudigel, H., Dilek, Y., de Wit, M., Van Kranendonk, M., and Schiffmann, P. (2008) Oceanic pillow lavas and hyaloclastites as habitats for microbial life through time—a review. In *Links between Geological Processes, Microbial Activities, and Evolution of Life,* Modern Approaches in Solid Earth Sciences Vol. 4, edited by Y. Dilek, H. Furnes, and K. Muehlenbachs, Springer, Dordrecht, pp 1–68.

Furnes, H., de Wit, M.J., Robins, B., and Sandståd, N.R. (2011) Volcanic evolution of the upper Onverwacht Suite, Barberton greenstone belt, South Africa. *Precambrian Res* 186:28–50.

Grosch, E.G. and McLoughlin, N. (2013) Paleoarchean sulfur cycle and biogeochemical surface conditions on the early

Earth, Barberton, South Africa. *Earth Planet Sci Lett* 377–378:142–154.

Grosch, E.G., McLoughlin, N., de Wit, M., and Furnes, H. (2009a) Drilling for the Archean roots of life and tectonic Earth in the Barberton Mountains. *Scientific Drilling* 8:24–28.

Grosch, E.G., McLoughlin, N., de Wit, M.J, and Furnes, H. (2009b) Deciphering Earth's deep history: drilling in Africa's oldest greenstone belt. *Eos* 90:350–351.

Grosch, E.G., Kosler, J., McLoughlin, N., Drost, K., Slama, J., and Pedersen, R.B. (2011) Paleoarchean detrital zircon ages from the earliest tectonic basin in the Barberton greenstone belt, Kaapvaal Craton, South Africa. *Precambrian Res* 191:85–99.

Grosch, E.G., Vidal, O., Abu-Alam, T., and McLoughlin, N. (2012) *PT* constraints on the metamorphic evolution of the Paleoarchean Kromberg type-section, Barberton greenstone belt, South Africa. *Journal of Petrology* 53:513–545.

Hanor, J.S. and Duchac, K.C. (1990) Isovolumetric silicification of early Archean komatiites: geochemical mass balances and constraints on origin. *J Geol* 98:863–877.

Hellevang, H., Huang, S., and Thorseth, I.H. (2010) The potential for low-temperature abiotic hydrogen generation and a hydrogen-driven deep biosphere. *Astrobiology* 11:711–724.

Hillier, S. and Velde, B. (1991) Octahedral occupancy and the chemical composition of diagenetic (low-temperature) chlorites. *Clay Miner* 26:146–168.

Hofmann, A. (2011) Archean hydrothermal systems in the Barberton greenstone belt and their significance as a habitat for early life. In *Earliest Life on Earth: Habitats, Environments and Methods of Detection*, edited by S.D. Golding and M. Glikson, Springer, Dordrecht, pp 51–77.

Hofmann, A. and Bolhar, R. (2007) Carbonaceous cherts in the Barberton greenstone belt and their significance for the study of early life in the Archean record. *Astrobiology* 7:355–388.

Hofmann, A. and Harris, C. (2008) Stratiform alteration zones in the Barberton greenstone belt: a window into subseafloor processes 3.5–3.3 Ga ago. *Chem Geol* 257:224–242.

Holland, T.J.B. and Powell, R. (1998). An internally-consistent thermodynamic dataset for phases of petrological interest. *Journal of Metamorphic Geology* 16:309–344.

Inoue, A., Meunier, A., Patrier-Mas, P., Rigault, C., Beaufort, D., and Viellard, P. (2009) Application of chemical geothermometry to low-temperature trioctahedral chlorites. *Clays Clay Miner* 57:371–382.

Izawa, M.R.M., Banerjee, N.R., Flemming, R.L., Bridge, N.J., and Schultz, C. (2010) Basaltic glass as a habitat for microbial life: implications for astrobiology and planetary exploration. *Planet Space Sci* 58:583–591.

Jiang, W.T., Peacor, D.R., and Buseck, P.R. (1994) Chlorite geothermometry contamination and apparent octahedral vacancies. *Clays Clay Miner* 42:593–605.

Lanari, P., Guillot, S., Schwartz, S., Vidal, O., Tricart, P., Riel, N., and Beyssac, O. (2012) Diachronous evolution of the alpine continental subduction wedge: evidence from *P-T* estimates in the Briançonnais Zone houillère (France—Western Alps). *Journal of Geodynamics* 56–57:39–54.

Lanari, P., Riel, N., Guillot, S., Vidal, O., Schwartz, S., Pêcher, A., and Hattori, K. (2013) Deciphering high-pressure metamorphism in collisional context using microprobe-mapping methods: application to the Stak eclogitic massif (NW Himalaya). *Geology* 41:111–114.

Lanari, P., Vidal, O., De Andrade, V., Dubacq, B., Lewin, E., Grosch, E.G., and Schwartz, S. (2014a) XMapTools: a MATLAB©-based program for electron microprobe X-ray image processing and geothermobarometry. *Comput Geosci* 62:227–240.

Lanari, P., Wagner, T., and Vidal, O. (2014b) A thermodynamic model for di-trioctahedral chlorite from experimental and natural data in the system MgO-FeO-Al_2O_3-SiO_2-H_2O: applications to *P-T* sections and geothermometry. *Contrib Mineral Petrol* 167:968.

Lever, M.A., Rouxel, O., Alt, J.C., Shimizu, N., Ono, S., Coggon, R.M., Shanks, W.C., III, Lapham, L., Elvert, M., Preito-Mollar, X., Hinrichs, K.U., Inagaki, F., and Teske, A. (2013) Evidence for microbial carbon and sulfur cycling in deeply buried ridge flank basalt. *Science* 399:1305–1308.

Lopez-Martinez, M., York, D., and Hanes, J.A. (1992) A $^{40}Ar/^{39}Ar$ geochronological study of komatiites and komatiitic basalts from the Lower Onverwacht volcanics: Barberton Mountain Land, South Africa. *Precambrian Res* 57:91–119.

Martin, C., Debaille, V., Lanari, P., Goderist, S., Vanhaecke, F., Vidal, O., and Claeys, P. (2013) REE and Hf distribution among mineral phases in the CV-CK clan: a way to explain present-day Hf isotopic variations in chondrites. *Geochim Cosmochim Acta* 120:495–513.

Mason, O.U., Nakagawa, T., Rosner, M., Van Nostrand, J.D., Zhou, J., Maruyama, A., Fisk, M.R., and Giovannoni, S.J. (2010) First investigation of the microbiology of the deepest layer of ocean crust. *PLoS One* 5:e15399.

McCollom, T.M. and Seewald, J.S. (2013) Serpentinites, hydrogen, and life. *Elements* 9:129–134.

McLennan, S.M., Sephton, M.A., Allen, C., Allwood, A.C., Barbieri, R., Beaty, D.W., Boston, P., Carr, M., Grady, M., Grant, J., Heber, V.S., Herd, C.D.K., Hoffman, B., King, P., Mangold, N., Ori, G.G., Rossi, A.P., Raulin, F., Ruff, S.W., Sherwood-Lollar, B., Symes, S., and Wilson, M.G. (2012) Planning for Mars returned sample science: final report of the MSR End-to-End International Science Analysis Group (E2E-iSAG). *Astrobiology* 12:175–230.

McLoughlin, N., Brasier, M.D., Perry, R.S., Wacey, D., and Green, O.R. (2007) On biogenicity criteria for endolithic microborings on early Earth and beyond. *Astrobiology* 7:10–11.

McLoughlin, N., Wacey, D., Kruber, C., Kilburn, M.R., Thorseth, I.H., and Pedersen, R.B. (2011) A combined TEM and NanoSIMS study of endolithic microfossils in altered seafloor basalt. *Chem Geol* 289:154–162.

McLoughlin, N., Grosch, E.G., Kilburn, M., and Wacey, D. (2012) Sulfur isotope evidence for a Paleoarchean subseafloor biosphere, Barberton, South Africa. *Geology* 40:1031–1034.

McMahon, S., Parnell, J., Ponicka, J., Hole, M., and Boyce, A. (2013) The habitability of vesicles in martian basalt. *Astronomy and Geophysics* 54:1.17–1.21.

Ménez, B., Pasini, V., and Brunelli, D. (2012) Life in the hydrated suboceanic mantle. *Nat Geosci* 5:133–137.

Michalski, J.R., Cuadros, J., Niles, P.B., Parnell, J., Rogers, A.D., and Wright, S.P. (2013) Groundwater activity on Mars and implications for a deep biosphere. *Nat Geosci* 6: 133–138.

Moyen, J.F., Stevens, G., and Kisters, A.F.M. (2006) Record of mid-Archaean subduction from metamorphism in the Barberton terrain, South Africa. *Nature* 44:559–662.

Muñoz, M., de Andrade, V., Vidal, O., Lewin, E., Pascarelli, S., and Susisi, J. (2006) X-ray absorption micro-mapping of iron redox and speciation in chlorite. *Geochemistry, Geophysics, Geosystems* 7, doi:10.1029/2006GC001381.

Oze, C. and Sharma, M. (2005) Have olivine, will gas: serpentinization and the abiogenic production of methane on Mars. *Geophys Res Lett* 32, doi:10.1029/2005GL022691.

Parnell, J., Bowden, S.A., Osinski, G.R., Lee, P., Green, P., Taylor, C.W., and Baron, M. (2007) Organic geochemistry of impactites from the Haughton impact structure, Devon Island, Nunavut, Canada. *Geochim Cosmochim Acta* 71:1800–1819.

Parnell, J., Boyce, A.J., and Blamey, N.J.F. (2010a) Follow the methane: the search for a deep biosphere, and the case for sampling serpentinites, on Mars. *International Journal of Astrobiology* 9:193–200.

Parnell, J., Boyce, A., Thackrey, S.N., Muirhead, D.K., Lindgren, P., Mason, C., Taylor, C.W., Still, J.W., Bowden, S.A., Osinski, G.R., and Lee, P. (2010b) Sulfur isotope signatures for rapid colonization of an impact crater by thermophilic microbes. *Geology* 38:271–274.

Peckmann, J., Bach, W., Behrens, K., and Reitner, J. (2008) Putative cryptoendolithic life in Devonian pillow basalt, Rheinisches Schiefergebirge, Germany. *Geobiology* 6:125–135.

Philippot, P., Van Kranendonk, M., Van Zuilen, M., Lepot, K., Rividi, N., Teitler, Y., Thomazo, C., Blanc-Valleron, M., Rouchy, J., Grosch, E.G., and de Wit, M.J. (2009) Drilling Archean hydrothermal and sedimentary settings of the Pilbara Craton, Western Australia and Barberton Belt, South Africa. *C R Palevol* 8:649–663.

Rouxel, O., Ono, S., Alt, J., Rumble, D., and Ludden, J. (2008) Sulfur isotope evidence for microbial sulfate reduction in altered oceanic basalts at ODP Site 801. *Earth Planet Sci Lett* 268:110–123.

Santelli, C.M., Orcutt, B.N., Banning, E., Bach, W. Moyer, C.L., Sogin, M.L., Staudigel, H., and Edwards, K. (2008) Abundance and diversity of microbial life in ocean crust. *Nature* 453:653–657.

Schulte, M., Blake, D., Hoehler, T., and McCollom, T. (2006) Serpentinization and its implications for life on the early Earth and Mars. *Astrobiology* 6:364–376.

Schumann, G., Manz, W., Reitner, J., and Lustrino, M. (2004) Ancient fungal life in North Pacific Eocene oceanic crust. *Geomicrobiol J* 21:241–246.

Squyres, S.W., Arvidson, R.E., Ruff, S., Gellert, R., Morris, R.V., Ming, D.W., Crumpler, L., Farmer, J.D., Des Marais, D.J., Yen, A., McLennan, S.M., Calvin, W., Bell, J.F., III, Clark, B.C., Wang, A., McCoy, T.J., Schmidt, M.E., and de Souza, P.A., Jr. (2008) Detection of silica-rich deposits on Mars. *Science* 320:1063–1067.

Squyres, S.W., Arvidson, R.E., Bell, J.F., III, Calef, F., III, Clark, B.C., Cohen, B.A., Crumpler, L.A., de Souza, P.A., Jr., Farrand, W.H., Gellert, R., Grant, J., Herkenhoff, K.E., Hurowitz, J.A., Johnson, J.R., Jolliff, B.L., Knoll, A.H., Li, R., McLennan, S.M., Ming, D.W., Mittlefehldt, D.W., Parker, T.J., Paulsen, G., Rice, M.S., Ruff, S.W., Schroder, C., Yen, A.S., and Zacny, K. (2012) Ancient impact and aqueous processes at Endeavour Crater, Mars. *Science* 336:570–576.

Staudigel, H., Furnes, H., McLoughlin, N., Banerjee, N.R., Connell, L.B., and Templeton, A. (2008) 3.5 billion years of glass bioalteration: volcanic rocks as a basis for microbial life? *Earth-Science Reviews* 89:156–176.

Thorseth, I.H., Torsvik, T., Furnes, H., and Muehlenbachs, K. (1995) Microbes play an important role in the alteration of oceanic crust. *Chem Geol* 126:137–146.

Vidal, O., Parra, T., and Trotet, F. (2001) A thermodynamic model for Fe-Mg aluminous chlorite using data from phase equilibrium experiments and natural pelitic assemblages in the 100–600°C, 1–25 kbar P-T range. *Am J Sci* 301:557–592.

Vidal, O., Parra, T., and Vieillard, P. (2005) Experimental data on the Tschermak solid solution in Fe-chlorites: application to natural examples and possible role of oxidation. *Am Mineral* 90:359–370.

Vidal, O., de Andrade, V., Lewin, E., Muñoz, M., Parra, T., and Pascarelli, S. (2006) P-T-deformation Fe^{3+}/Fe^{2+} mapping at the thin section scale and comparison with XANES mapping: application to a garnet-bearing metapelite from the Sambagawa metamorphic belt (Japan). *Journal of Metamorphic Geology* 24:669–683.

Walsh, M.M. (1992) Microfossils and possible microfossils from the Early Archean Onverwacht Group, Barberton Mountain Land, South Africa. *Precambrian Res* 54:271–293.

Westall, F., de Ronde, C.E.J., Southham, G., Grassineau, N., Colas, M., Cockell, C., and Lammer, H. (2006) Implications of a 3.472–3.333 Ga-old subaerial microbial mat from the Barberton greenstone belt, South Africa for the UV environmental conditions on the early Earth. *Philos Trans R Soc Lond B Biol Sci* 361:1857–1875.

Westall, F., Foucher, F., Cavalazzi, B., de Vries, S.T., Nijman, W., Pearson, V., Watson, J., Verchovsky, A., Wright, I., Rouzaud, J.-N., Marchesini, D., and Anne, S. (2011) Volcaniclastic habitats for early life on Earth and Mars: a case study from ~3.5 Ga-old rocks from the Pilbara, Australia. *Planet Space Sci* 59:1093–1106.

Address correspondence to:
Eugene G. Grosch
Department of Earth Science and Centre for Geobiology
University of Bergen
Norway N-5007

E-mail: geogene@gmail.com

Submitted 1 November 2013
Accepted 28 January 2014